A Model Comparison: Numerical Simulations of the North and Equatorial Atlantic Oceanic Circulation in Depth and Isopycnic Coordinates

ERIC P. CHASSIGNET, LINDA T. SMITH, AND RAINER BLECK

RSMAS/MPO, University of Miami, Miami, Florida

FRANK O. BRYAN

NCAR/CGD, Boulder, Colorado

(Manuscript received 5 December 1995, in final form 13 March 1996)

ABSTRACT

A series of medium-resolution (~1°) numerical simulations for the equatorial and North Atlantic basin have been performed with two primitive equation models, one employing depth and the other density as the vertical coordinate. The models have been configured for this exercise in as similar a fashion as their basic formulations allow, and with fundamentally identical initialization, boundary conditions, and forcing functions for each of the experiments. The purpose of comparing the models' results is twofold: 1) to understand the degree to which model-generated circulation fields depend on the particular model architecture by examining the rate of divergence of the solutions of an isopycnic and a depth coordinate model given the same initial conditions and 2) to uncover and remedy possible defects in either model design. The comparison is focused on the importance in each simulation of the choice of mixing parameterization, which has a crucial impact on the meridional overturning circulation, on the associated northward heat transport, and on the evolution of water masses. Although the model-generated horizontal fields viewed at specific times during the integrations do not appear to be strongly dependent on the design of each model and are in good agreement with one another, the integrated properties of the depth coordinate model and the isopycnic coordinate model diverge significantly over time, with the depth coordinate model being unable to retain its most dense water masses after long integration periods.

1. Introduction

Before the Navier–Stokes differential equations can be solved numerically, they must be converted into an algebraic system, a conversion process which entails numerous approximations. Numerical models have improved over the years not only because of a better physical understanding, but also because modern computers permit a more faithful representation of the differential equations by their algebraic analogs. Specifically, the discretization or "truncation" error introduced when approximating differentials by finite differences or Galerkin methods decreases as advances in computing speed and memory allow smaller and smaller mesh sizes.

Rather than relying upon the development of computers that ultimately will allow the solutions of algebraic and differential equations to converge, numerical modelers try to reduce the truncation error in their models on existing machines by using sophisticated ("higher order") approximations or by distributing a fixed number of grid points in physical space such that they optimally define the spatial structure of the modeled system. One method of reducing the truncation error in geophysical fluid modeling entails replacing the independent variable z in the governing equations by a different coordinate (sigma, density, . . .).

Mixing in turbulent stratified fluids where buoyancy effects play a role takes place predominantly along isopycnic or constant potential density surfaces (Iselin 1939; Montgomery 1940; McDougall and Church 1986). If the conservation equations for salt and temperature are discretized in x, y, z space, that is, if the three-dimensional vectorial transport of these quantities is numerically evaluated as the sum of scalar transports in x, y, z direction, experience shows that it is virtually impossible to avoid diffusion of the transported variables in those three directions (Veronis 1975; Redi 1982, hereafter referred to as R82; Cox 1987; Gent and McWilliams 1990, hereafter referred to as GM90; Gent et al. 1995). Thus, regardless of how the actual mixing term in the conservation equations is formulated, numerically induced mixing is likely to have a cross-isopycnal ("diapycnal") component that may well overshadow the common diapycnal processes that occur in nature. This leads to serious errors in long-

Corresponding author address: Dr. Eric P. Chassignet, RSMAS, University of Miami, 4600 Rickenbacker Causeway, Miami, FL 33149.
E-mail: echassignet@rsmas.miami.edu

term climate simulations (Toggweiler 1994; Böning et al. 1995).

Isopycnic coordinate modeling seeks to eliminate this type of truncation error by reversing the traditional role of depth as an independent variable and (potential) density as a dependent variable. The dynamic equations are transformed from x, y, z to x, y, ρ coordinates and are discretized on an x, y, ρ model grid, where ρ here is the potential density. Transport in x, y direction then takes place in the model on isopycnic surfaces, and the associated numerical diffusion has no diapycnal component. Transport in z direction translates into transport along the ρ axis and can be entirely suppressed if so desired; that is, it has no unwanted diapycnal component. As a result, spurious heat exchange between warm surface waters and cold abyssal waters and horizontal heat exchange across sloping isopycnals such as those marking frontal zones are minimized in isopycnic models. Potential density surfaces are not, however, neutral surfaces (McDougall and Church 1986) and dianeutral fluxes may be present when potential density is used as the vertical coordinate. The remedy is to take into account the compressibility of sea water in the equation of state.

While a vertical discretization in ρ has obvious advantages in idealized models of adiabatic, mechanically driven flow, where it eliminates the need to solve a thermodynamic equation, the payoff is less clear in ocean models that treat density as a function of the three independently forced prognostic variables: temperature, salinity, and pressure. Nevertheless, the argument has been made that of all numerical schemes used for transporting thermodynamic variables in three-dimensional ocean models, those using isopycnic discretization will come closest to accomplishing the transport without introducing spurious diabatic effects (Bleck et al. 1992).

It is fair to say that there is no "best" choice of vertical coordinate in a geophysical fluid model since, as already mentioned, the solutions of the discretized finite-difference equations should all converge toward the solutions of the corresponding differential equations as mesh size goes to zero. Each coordinate system is afflicted with its own set of truncation errors, the implications of which must be understood and prioritized. Finally, the success of any simulation is, at the present time, directly dependent upon the choices that are made for the parameterization of various subgrid processes. These choices depend directly on the overall model architecture and may be more or less natural to the particular model design.

This paper describes results obtained from a basin-wide comparison of a series of medium resolution experiments ($\sim 1°$ grid spacing) performed with two primitive equation numerical models, the depth coordinate model developed at the Geophysical Fluid Dynamics Laboratory (GFDL) and the Miami Isopycnic Coordinate Ocean Model (MICOM). The purpose of the comparison is twofold: 1) to understand the degree to which model-generated circulation fields depend on the particular model architecture by examining the rate of divergence of the solutions of an isopycnic and a depth coordinate model, given the same initial conditions, and 2) to uncover and remedy possible defects in either model design. Another comparison exercise between the same two models was recently performed by Roberts et al. (1996) and Marsh et al. (1996) for a different configuration. In this paper, the focus is on the relative importance of the mixing parameterization on water mass evolution as a function of model architecture. This parameterization has recently been shown to have a crucial impact on the meridional circulation and heat transport in depth coordinate models (Böning et al. 1995). This paper emphasizes model–model comparison aspects as extensive model–data comparisons have already been performed with both numerical models (Böning et al. 1995, 1996; Bryan et al. 1995a; New et al. 1995).

This work is part of the WOCE Community Modeling Effort (CME), a multiyear, multi-institutional series of model applications and analyses, with the goal of establishing a sequence of baseline calculations of the wind- and thermohaline-driven large-scale ocean circulation. Important component activities of the CME include the design and execution of the benchmark simulations themselves, analysis of the results, and comparison with observations (U.S. WOCE Office 1993).

The layout of the paper is the following. In section 2, the models' configurations and differences in setup are described. Section 3 presents horizontal flow patterns and vertical cross sections from each model's results. The different ventilation patterns are discussed in detail in section 4. Section 5 investigates the sensitivity of the meridional overturning cell and associated heat transport to boundary conditions and mixing. In section 6, the time evolution of the different water masses is presented and discussed. Finally, the results are summarized and discussed in the concluding section.

2. The numerical experiments

a. The numerical models and their configuration

Both numerical models are well documented in the literature. For a review of the GFDL model, the reader is referred to Cox (1984), and for MICOM, to Bleck and Chassignet (1994). The first series of CME experiments was performed in the late 1980s for the North and Equatorial Atlantic Ocean basin at the National Center for Atmospheric Research (NCAR) (Bryan and Holland 1989; Holland and Bryan 1994a,b; Bryan et al. 1995a) and at the Institut für Meereskunde (Böning et al. 1991a,b; Böning and Budich, 1992; Beckman et al. 1994).

The computational domain is the equatorial and North Atlantic Ocean basin from 15°S to 65°N, includ-

ing the Caribbean Sea and the Gulf of Mexico, but excluding the Mediterranean Sea. The bottom topography is derived from a digital terrain dataset with 5′ latitude–longitude resolution. A Kraus–Turner mixed layer parameterization is included. All surface boundary conditions are based on seasonal climatological datasets. The wind stress and wind work values are taken from the Hellerman and Rosenstein (1983) climatology. The surface thermal boundary conditions are specified by a linear bulk formula described by Han (1984), while those for freshwater flux are implemented in traditional fashion as a linear relaxation of the surface salinity toward the Levitus (1982) climatology. Open ocean boundaries are treated as closed, but are outfitted with buffer zones in which the temperature T and salinity S are linearly relaxed toward their seasonally varying climatological values. These buffer zones restore the T and S fields to the Levitus climatology in order to approximately recover the vertical shear of the currents through geostrophic adjustment. The four buffer zones are located at the northern boundary and at the southern boundary (4° latitude band), in the northwestern corner (representing the Labrador Sea), and in the Gulf of Cadiz (representing the Mediterranean Sea) (Fig. 1). The restoring timescale for the boundaries varies linearly from 25 days at the inner edge to 5 days at the walls. The timescale for the Labrador Sea region is 25 days, and for the Mediterranean, 1 year. For more details, the reader is referred to Bryan and Holland (1989) and Holland and Bryan (1994a,b).

MICOM's configuration was made as close as possible to that of the original GFDL experiment performed at NCAR so that the models could be compared on equal terms, meaning that they are as similar as their formulations allow. Because of the intrinsic nature of the numerical approaches, there are some differences in setup. They are the following:

1) Horizontal grid: The GFDL code uses a B grid with a resolution of 1° in latitude and 1.2° in longitude. In MICOM, the model equations are solved on a C grid forming a regular mesh on a Mercator projection with the north–south grid lines corresponding to meridians spaced 0.9° apart.

2) Vertical grid: In both models, the vertical grid was chosen to provide maximum resolution in the upper part of the ocean. In the GFDL model, 30 discrete levels are used with a spacing of 35 m at the surface, gradually increasing to 250 m by 1000 m depth. Below 1000 m, the spacing is a constant 250 m. MICOM includes a total of 16 layers: a Kraus–Turner-type mixed layer (vertically homogeneous, but of density varying in the horizontal) and 15 isopycnic layers with potential density (σ_θ) values of 24.7, 25.28, 25.77, 26.18, 26.52, 26.80, 27.03, 27.22, 27.38, 27.52, 27.64, 27.74, 27.82, 27.88, and 27.92.

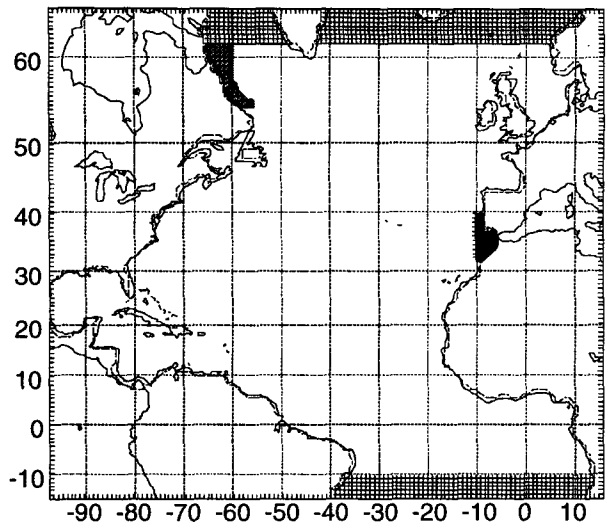

FIG. 1. Model domain. The dotted areas indicate the location and size of the buffer zones in which temperature and salinity are relaxed to climatological values (light: northern and southern boundaries, medium: Labrador Sea, dark: Mediterranean outflow).

3) Freshwater flux: Matching the prescription of surface freshwater flux in terms of a surface salinity relaxation toward Levitus (1982) climatology was a nontrivial matter. Relaxing salinity in the upper 35 m of the water column, as in the GFDL model, is not feasible in the isopycnic model whose uppermost layer may vary in depth between 20 and several thousand meters. The chosen procedure computes a surface salinity flux corresponding to the effect the relaxation term would have on the salinity in the uppermost 35 m and uses this flux to compute salinity tendencies in MICOM's variable depth mixed layer.

b. Initial conditions and integration time

All experiments were initialized with T and S for January conditions from the Levitus (1982) climatology. In the MICOM runs, the Levitus dataset had to be transformed to a piecewise constant (stairsteplike) vertical density profile for the model initialization and buffer zones. Static instabilities present in the original data had to be removed, and a transform scheme preserving the vertically integrated density in each grid column had to be developed.

The comparison was complicated by the fact that the experiments performed with the GFDL model were first integrated for more than 100 years using the acceleration technique of Bryan (1984), in which tracers and momentum are integrated asynchronously. This acceleration permits the thermohaline circulation to reach an equilibrium state relatively quickly. Following this, several decades of synchronous integrations were then performed. For a meaningful comparison, one MICOM experiment was initialized with model data from one

TABLE 1. Parameters of the experiments. For all experiments; the quadratic bottom drag coefficient is 1.3×10^{-3}. R82: see text; GM90: see text.

Experiment	A_{MH} ($m^2 s^{-1}$)	A_{MV} ($m^2 s^{-1}$)	A_{DH} ($m^2 s^{-1}$)	A_{DV} ($m^2 s^{-1}$)
NCAR-1	1×10^4	3×10^{-3}	R82	3×10^{-5}
NCAR-2	1×10^4	3×10^{-3}	2×10^3	3×10^{-5}
NCAR-3	1×10^4	3×10^{-3}	GM90	3×10^{-5}
MIAMI-1	1×10^4	0	2×10^3	3×10^{-5}
MIAMI-2	1×10^4	0	2×10^3	3×10^{-5}
MIAMI-3	1×10^4	0	2×10^3	0
MIAMI-4	1×10^4	0	2×10^3	3×10^{-5}

of the accelerated physics NCAR integrations (see the description of the experiments in the next subsection for details).

c. *Mixing parameterization*

To investigate the effects of mixing in both numerical models, several experiments were considered. The mixing coefficients for the Laplacian operator are given in Table 1 for each experiment and are defined as A_{MH} (horizontal) and A_{MV} (vertical) for the momentum equations and A_{DH} (horizontal) and A_{DV} (vertical) for the tracer equations.

- *NCAR-1:* Base experiment. The diffusion for the tracers is formulated as described by R82 and is based on the rotation of the diffusive flux vector to a coordinate locally tangent to an isopycnal surface. The scheme was implemented with depth-dependent isopycnal diffusivities (2×10^3 $m^2 s^{-1}$ in the upper ocean and 5×10^2 $m^2 s^{-1}$ in the deep ocean) and a background horizontal diffusivity (necessary to control numerical noise on the grid scale) of 1×10^2 $m^2 s^{-1}$.
- *NCAR-2:* As NCAR-1 except that the horizontal diffusion is formulated as a traditional Laplacian operator [EXP 12.0 in Holland and Bryan (1994a) and Böning et al. (1995)].
- *NCAR-3:* As NCAR-1 except initialized from year 240 of NCAR-1, and with the parameterization of the effect of mesoscale eddies on the transport of tracers implemented as in GM90 [EXP 26.0 in Böning et al. (1995)] with an isopycnal diffusivity coefficient of 1×10^3 $m^2 s^{-1}$. This scheme was originally introduced by GM90 and Gent et al. (1995) as representing the down-gradient flux of thickness along isopycnals ("bolus" transport) corresponding to the dynamical effect of available potential energy and momentum transfers during baroclinic instabilities (Holland and Rhines 1980). The GM90 scheme also accounts for the eddy-induced advection, resulting from the difference between velocities averaged in time on either a horizontal surface or on an isopycnal surface, which has recently been termed the temporal-residual-mean (TRM) velocity by McDougall and McIntosh (1996, manuscript submitted to *J. Phys. Oceanogr.*).
- *MIAMI-1:* Same configuration as NCAR-1. Isopycnal and diapycnal mixing for the momentum and tracer equations are as displayed in Table 1. The coefficient for the smoothing of the isopycnal surfaces is 1×10^3 $m^2 s^{-1}$, and the resulting down-gradient flux of thickness is equivalent to the GM90 implementation of the eddy-induced circulation (T. J. McDougall 1996, personal communication).
- *MIAMI-2:* As MIAMI-1 except no restoring to Levitus (1982) in the Labrador Sea.
- *MIAMI-3:* As MIAMI-1 except no diapycnal mixing.
- *MIAMI-4:* As MIAMI-1 except initialized from year 220 of NCAR-1.

3. Horizontal flow patterns

In this section, a general description of the model horizontal flow patterns is presented, and the ventila-

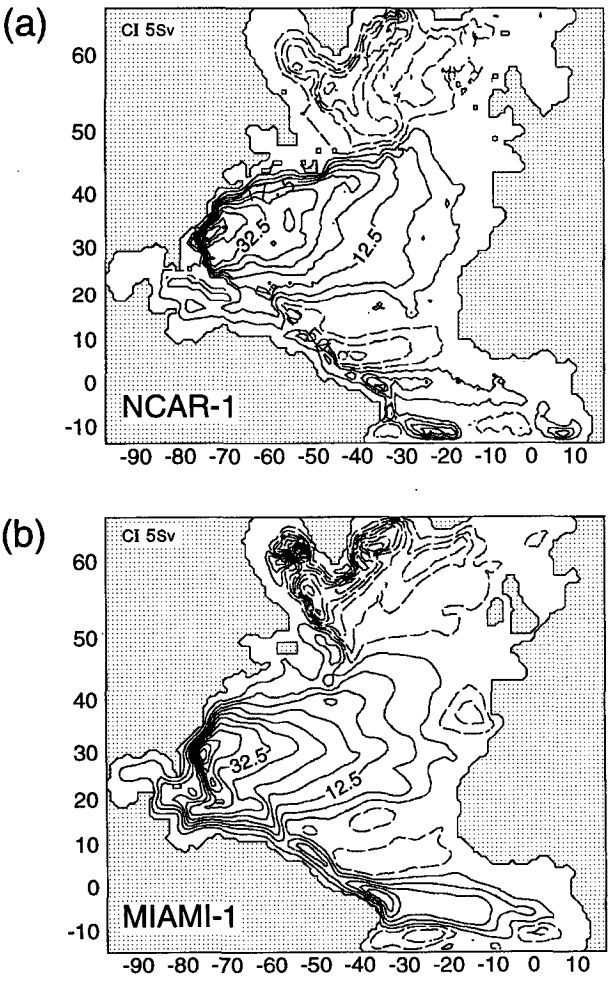

FIG. 2. Barotropic streamfunctions from NCAR-1 and MIAMI-1 for January (year 220 and 20, respectively). Contour interval (CI) of 5 Sv.

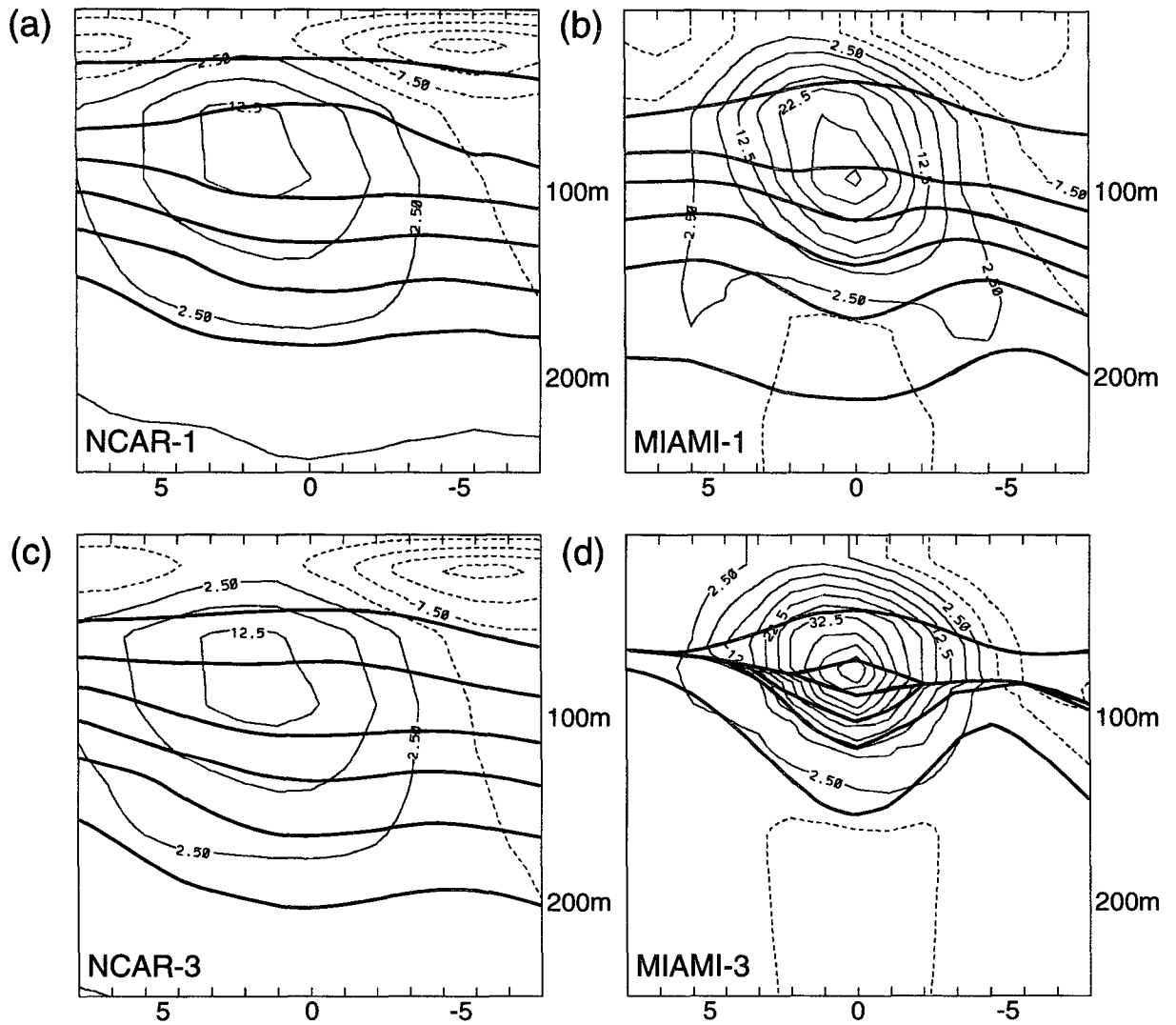

FIG. 3. Meridional cross section at 30°W in March (year 220 for NCAR-1; year 284 for NCAR-3; year 20 for MIAMI-1 and MIAMI-3). Velocity contours (CI = 5 cm s^{-1}) are superimposed on the layer interfaces defining the layers corresponding to the σ_θ given in section 2.

tion of the subtropical gyre is explored. The surface circulation focus will be on a few specific geographic areas such as the western boundary and equatorial regions. For display and comparison purposes, the NCAR results have been transformed to the x, y, ρ coordinate space (piecewise constant vertical density profile) of MICOM.

a. Barotropic streamfunction

Instantaneous barotropic streamfunctions from the NCAR-1 and MIAMI-1 runs for January are displayed in Fig. 2 for the entire domain. While the general patterns are in agreement, the MIAMI-1 results (Fig. 2b) exhibit a stronger subpolar gyre and a higher transport through the Straits of Florida. That transport has a magnitude of ~2.5 Sv (1 Sv $\equiv 10^6$ m^3 s^{-1}) in NCAR-1 and of ~12.5 Sv in MIAMI-1. These figures amount, respectively, to only approximately one-twelfth and one-third of the 30 Sv annual mean observed throughflow (Schott et al. 1988).

We attribute the difference in the Straits of Florida transport between the two models to the grid choices and to the manner in which each configuration deals with the bottom topography. In the B grid, used in the GFDL model, velocities are computed only at levels above the minimum depth of the four surrounding scalar grid points. Between Cuba and Florida, because of the coarse grid and shallow topography, the velocities are actually computed at the top two z levels only. In the C grid, velocities are computed at levels above the minimum depth of two neighboring grid points. The configuration in MIAMI-1 between Cuba and Florida

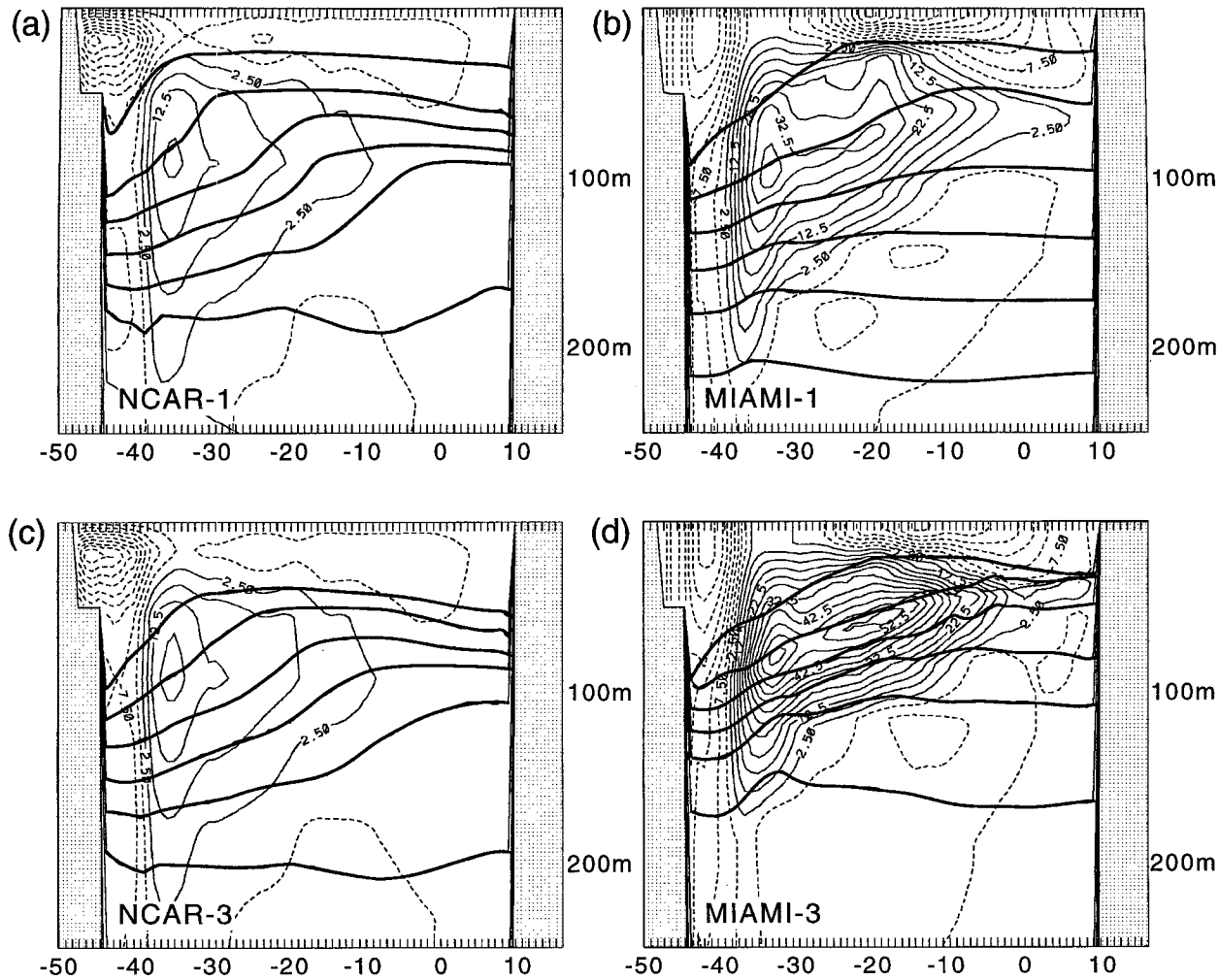

FIG. 4. Zonal cross section at the equator in March (year 220 for NCAR-1, year 284 for NCAR-3, year 20 for MIAMI-1 and MIAMI-3). Velocity contours (CI = 5 cm s^{-1}) are superimposed on the layer interfaces defining the layers corresponding to the σ_θ given in section 2.

is such that 13 layers have nonzero velocities, therefore allowing the greater transport through the straits.

Both the NCAR and MIAMI simulations exhibit a northward shift of the point of Gulf Stream separation from the coast as compared to observations (Fig. 2). A number of theories have been proposed concerning the incorrect separation latitude commonly seen in large-scale coarse-resolution diabatic ocean models [see McWilliams (1996) for a review]. Recent encouraging results in this regard have been reported by Bleck et al. (1995), who obtain a realistic separation of the Gulf Stream by following a medium resolution 13-year spinup experiment with a two-year integration of MICOM on a very fine horizontal mesh (0.08° longitude, less than 10 km), illustrating the importance of a highly inertial boundary layer.

The North Atlantic Current is seen to follow a more zonal path in NCAR-1 as compared to MIAMI-1, as similarly noted in the model comparison study of Roberts et al. (1996). They speculate that in the GFDL model, the zonality of the current is due in part to the formation of a vertically homogeneous water mass in the subpolar gyre, resulting from overflow mixing rather than from locally surface-induced convection, which prevents a deepening of the mixed layer in that region. In both NCAR-1 and MIAMI-1, part of the North Atlantic Current is diverted to feed the East Greenland Current (Fig. 2). This is contrary to the observed path and, as pointed out by Klinck (1995), may result in part from the fact that Iceland is located in the middle of the northern buffer zone. The modeled flow cannot follow the natural route into the Norwegian Sea from the North Atlantic around the north side of Iceland before emerging at the Denmark Strait.

The barotropic streamfunctions of the other NCAR and MIAMI experiments (Table 1) are very similar to those of the respective base experiments and are therefore not discussed. The overall agreement of the baro-

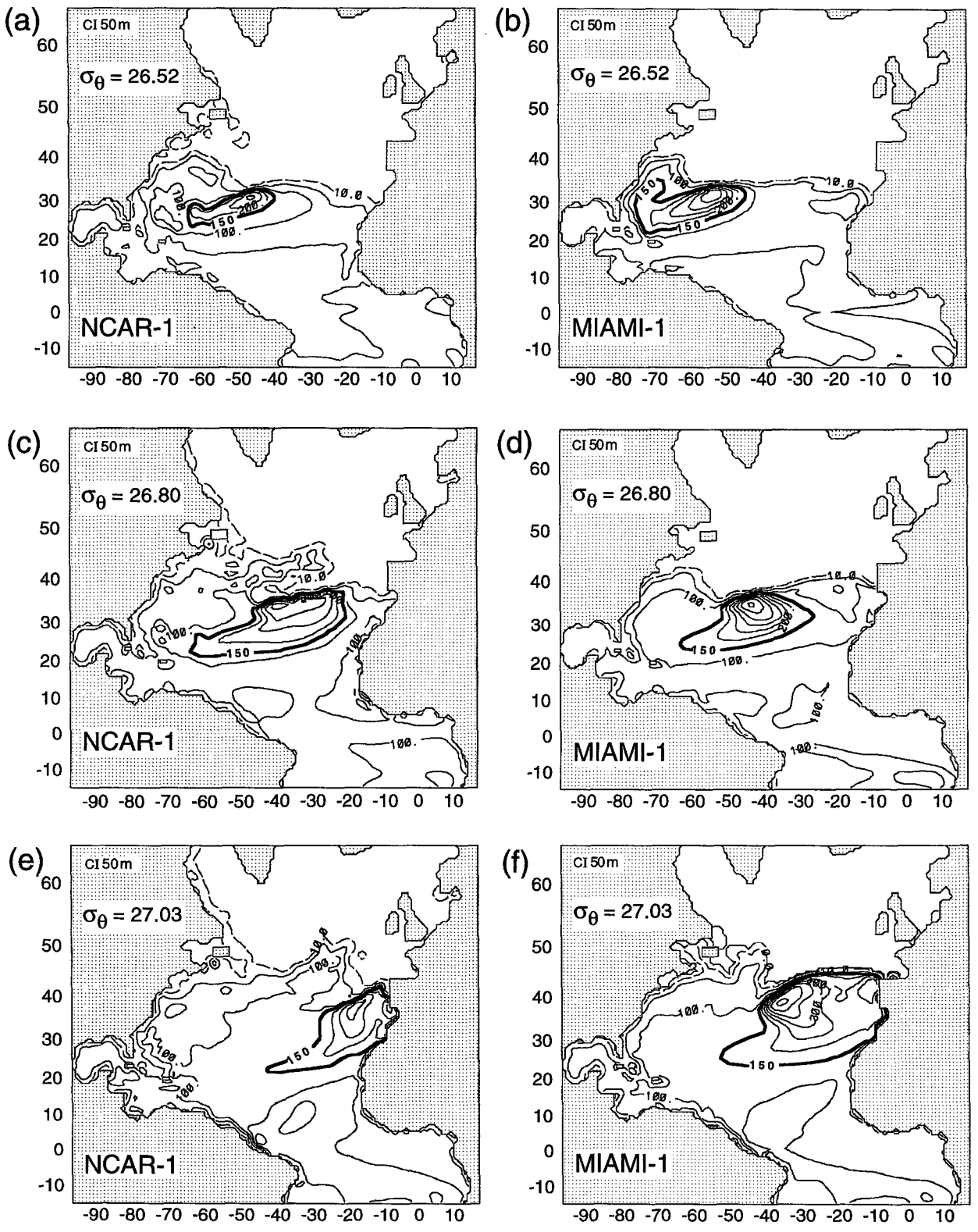

FIG. 5. Layer thickness (σ_θ = 26.52, 26.80, 27.03, respectively) for NCAR-1 (year 220) and MIAMI-1 (year 20) in March. The dashed line indicates the outcrop into the mixed layer while the heavy line is the 150-m contour. CI = 50 m.

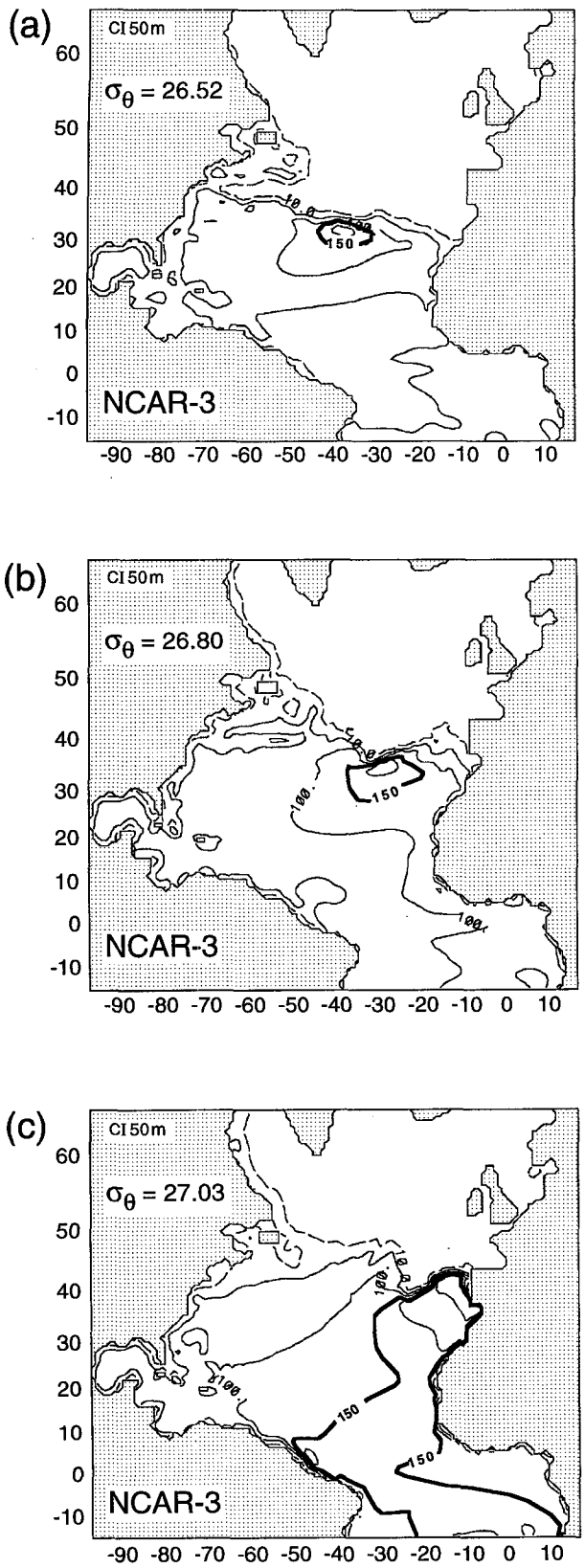

FIG. 6. As in Fig. 5 but for NCAR-3 (year 284).

tropic solutions among all experiments is not too surprising in the subtropical gyre, where one expects the Sverdrup balance to hold and the vertical discretization and associated mixing to be of minimal importance. However, greater differences might have been expected in the western boundary current region and in the subpolar gyre where higher order effects [joint effect of baroclinicity and relief (JEBAR), mixing, mixed layer physics, . . .] become important (Bryan et al. 1995a) and where weak stratification leads to vertical resolution problems in an isopycnic coordinate framework.

b. Equatorial undercurrent

The equatorial undercurrent (EUC) arises as a result of the replacement of fluid drawn into the equatorial mixed layer through Ekman suction by meridionally converging upper thermocline water. In most numerical simulations to date, the EUC and the associated upwelling system are not modeled properly (Wacongne 1989; Blanke and Delecluse 1993; Bryan et al. 1995b). In particular, the extent and strength of the modeled EUC depend strongly on the details of the initial stratification and on the turbulent vertical mixing scheme (Blanke and Delecluse 1993; Schott and Böning 1991). In both NCAR-1 and MIAMI-1, the EUC is a robust feature. Figure 3a shows one example of the EUC in the NCAR-1 run for the month of March along 30°W (close to the point of EUC maximum velocity). The current has a meridional extent of about 900 km, a vertical extent of less than 200 m, and a core velocity of about 0.15 m s^{-1}. That speed is significantly less than suggested by observations, namely, a core velocity on the order of 0.80 m s^{-1} [given by Garzoli and Katz (1983) as a 5-month average at 23.5°W]. A corresponding section through model fields from the MIAMI-1 run is shown in Fig. 3b. The core velocity, ~0.30 m s^{-1}, is roughly double that seen in the NCAR-1 results. In both NCAR-1 and MIAMI-1, the maximum core velocity is located at ~35°W (Figs. 4a,b).

In addition to the core speed, differences between the EUC representation in the two numerical models can be found in the extent of the undercurrent's eastward penetration and in the latitudinal position of the core. The zonal penetration of the EUC is significantly greater in MIAMI-1, where the current extends nearly to the African coast (Fig. 4b). The core of the EUC in March for NCAR-1 is located on the average 1° north of the equator. In MIAMI-1, the core is located 1° north of the equator at ~35°W, at the equator at 30°W, and ~1° south of the equator to the east of 30°W. In both NCAR-1 and MIAMI-1, no significant latitudinal displacement of the core is observed as a response to the seasonal variations in meridional wind stress. However, a better representation of the equatorial dynamics is observed in the higher resolution CME simulations (Schott and Böning 1991; Bryan et al. 1995b) where an annual cycle in the EUC location is quite pronounced.

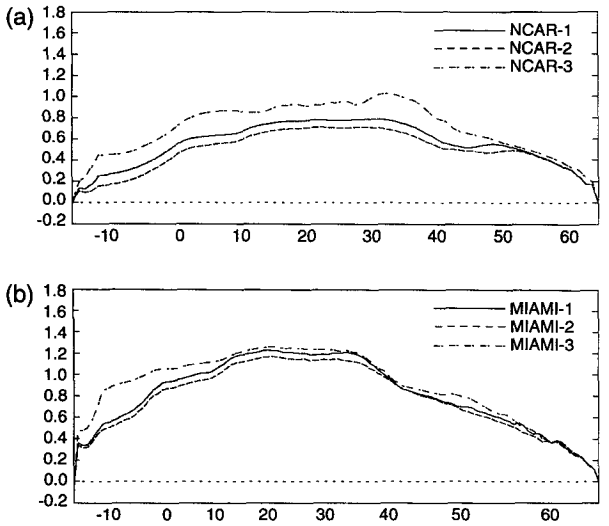

FIG. 7. Annual mean meridional heat transport (petawatts) for the NCAR and MIAMI experiments.

Adoption of the GM90 eddy mixing scheme in NCAR-3 (Figs. 3c, 4c) has a negligible effect on the structure and strength of the EUC when compared to the structure in NCAR-1 obtained with the R82 horizontal diffusion (Fig. 3a). This is not unexpected in a region such as the EUC (Fig. 3a,c), where isopycnals are nearly level and where GM90 does not play a strong role. Diapycnal mixing, however, as pointed out by Schott and Böning (1991) and Bryan et al. (1995b), is an important factor in controlling the EUC strength. This is demonstrated in MIAMI-3 where the omission of diapycnal mixing induced a packing of the isopycnal layer interfaces (Fig. 3d), an EUC maximum core velocity of ~ 0.60 m s^{-1} (twice that of MIAMI-1), and an eastward penetration of the core all the way to the African continent (Fig. 4d).

c. *Ventilation patterns of the subtropical gyre*

Formation rates of different water masses are an important measure of a numerical model's ability to correctly represent the various physical processes at work. Of particular interest is the ventilation of the North Atlantic subtropical gyre, where large quantities of water are subducted. In this section, only the ventilation patterns established by the end of each model run are discussed and compared. For a discussion of their time evolution, the reader is referred to New et al. (1995) and Williams et al. (1995).

The ventilation of the subtropical gyre is governed by the existence of areas of strong subduction rates along the southern flank of the deep winter mixing region, where the southward Sverdrup flow carries water away from the base of the winter mixed layer as in the idealized thermocline model of Luyten et al. (1983). Subduction occurs for only a few of the interior layers, namely, those that come directly in contact with the winter mixed layer. For the 16-layer configuration used in MICOM, layers 5 to 9 (σ_θ range 26.18–27.2) are involved in the ventilation process, while the shallower and deeper layers are essentially inactive in this regard. We concentrate on three of these layers (6, 7, 8, with σ_θ = 26.52, 26.80, 27.03, respectively) for purposes of display. (Recall that the NCAR results have been transformed to the x, y, ρ coordinate space of MICOM.)

The thicknesses of layers 6 to 8 for NCAR-1 and for MIAMI-1 are displayed in Fig. 5. (The mixed layer depth for the NCAR results was computed by assuming that a potential density jump of $0.01\sigma_\theta$ units defines the bottom of the layer.) In both runs, there is a clear pattern of ventilation as evidenced by the closed thickness contours present in each layer (Fig. 5). These closed thickness contours (or mode water lenses) represent the amount of fluid that has irreversibly left the mixed layer to enter the permanent pycnocline (New et al. 1995) and are reminiscent of the subduction patterns of idealized thermocline models (Luyten et al. 1983; Williams et al. 1995) and of observations (Marshall et al. 1993; Qiu and Huang 1995). The lenses show a regular spatial progression, with lighter waters ventilating the western part of the domain and heavier waters the eastern part. The ventilation pattern for each layer strongly depends on the properties of the late-winter mixed layer, with an eastward (westward) shift of the ventilation source corresponding to a decrease (increase) in the wintertime mixed layer density (New et al. 1995). These patterns are in reasonable agreement with ob-

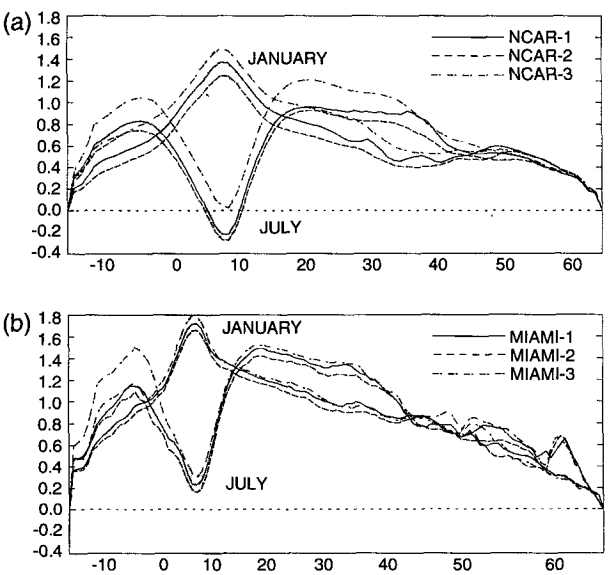

FIG. 8. Meridional heat transport (petawatts) for the NCAR and MIAMI experiments in January and July.

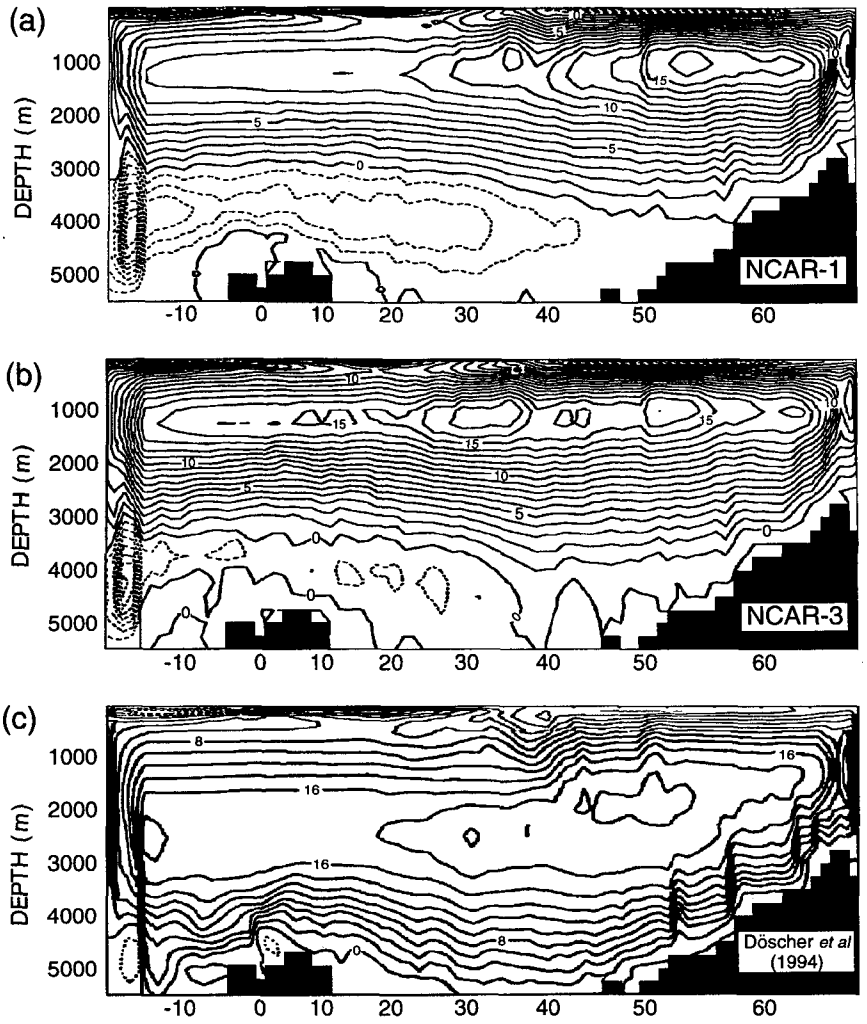

FIG. 9. Annual mean meridional overturning streamfunction for NCAR-1, NCAR-3, and experiment C2 of Döscher et al. (1994). CI = 1 Sv for NCAR-1 and NCAR-3; CI = 2 Sv for the Döscher et al. (1994) experiment.

served water mass distributions, such as the subtropical (or 18°C) mode water with potential density $\sigma_\theta \sim 26.5$ found in the Sargasso Sea and the heavier mode water (σ_θ range 27.0–27.3) observed northeast of the Azores (McCartney and Talley 1982). However, the thickness gradient of these mode water lenses differs substantially in the two model experiments, with the MIAMI-1 results displaying thicker ventilation cores (Fig. 5).

The impact of the GM90 parameterization is quite substantial as illustrated by Fig. 6 for NCAR-3. The core of the ventilated zones is seen to be considerably thinner than in NCAR-1, and the eastward displacement of the ventilation pattern suggests that the late-winter mixed layer is lighter (i.e., warmer or fresher) in NCAR-3 than in NCAR-1. As discussed by New et al. (1995), the evolution of the potential vorticity of the mode water lenses is governed by the diffusion of layer thickness. The GM90 parameterization includes mixing along isopycnal surfaces of the thickness between isopycnal surfaces, which appears to reduce the ventilation core intensity. Diapycnal mixing, on the other hand, is shown in MICOM to be of minor importance to the ventilation patterns, as only very small differences in this regard are observed between MIAMI-1 and MIAMI-3 (not illustrated). This is not unexpected considering the short Lagrangian timescales (several months) associated with the ventilation process in comparison to the timescale associated with diapycnal mixing (several decades).

4. Meridional heat transport and associated overturning cell

Of great interest to climate modeling is the sensitivity of the meridional heat transport and the associated

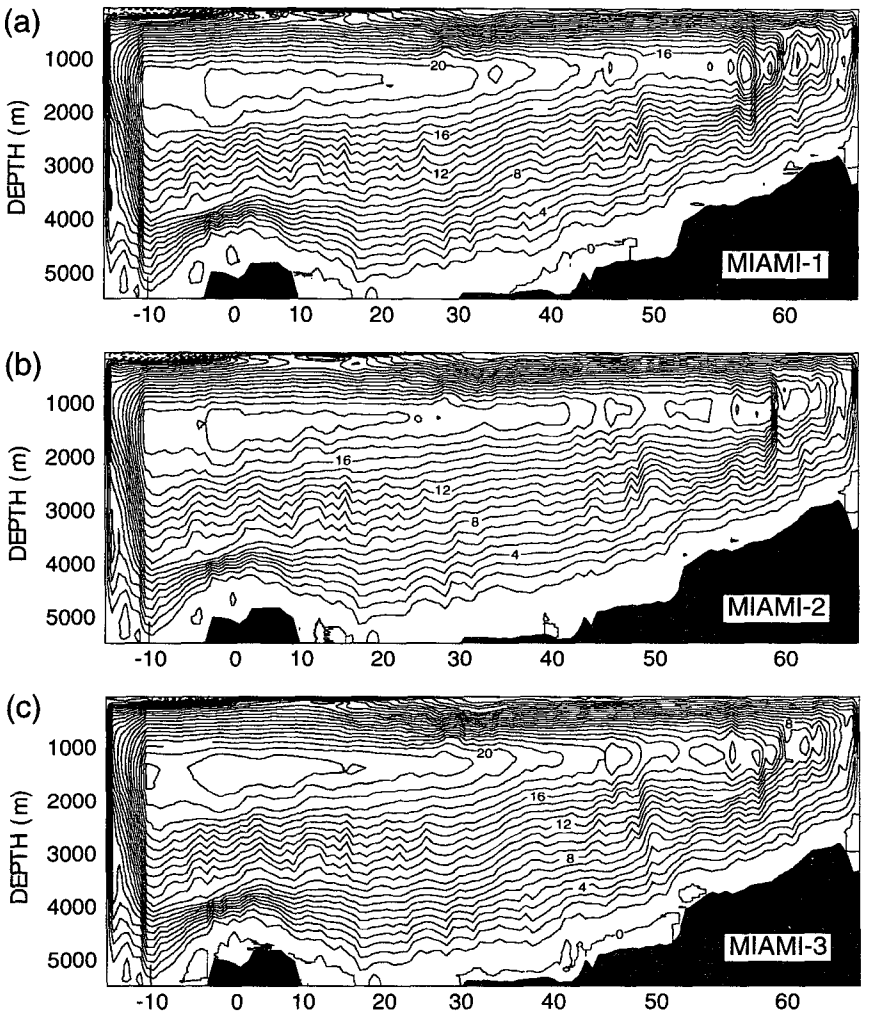

FIG. 10. Annual mean meridional overturning streamfunction for MIAMI-1, MIAMI-2, and MIAMI-3. CI = 1 Sv.

overturning cell to the model choice of mixing and boundary conditions. This particular aspect of the results is addressed in this section for model runs with different mixing parameterizations and buffer zones.

a. Meridional heat transport

The meridional heat transport is presented in Figs. 7a,b for the NCAR and MIAMI experiments, respectively. The maximum annual mean heat transport in the NCAR experiments is about 1 petawatt (PW) in NCAR-3 across ~25°N. This is in reasonable agreement with observed values that put the heat transport across 25°N at ~1.2 PW (Bryden and Hall 1980). The importance of the mixing parameterization in regard to the meridional heat transport is illustrated by NCAR-1 and NCAR-2, which, in the absence of the GM90 eddy-mixing parameterization, exhibit a significantly weaker transport (maximum 0.7 PW). As stated by Böning et al. (1995), the influence of the R82 mixing scheme (NCAR-1), when compared to the traditional horizontal Laplacian mixing (NCAR-2), is very small and does not significantly affect the heat transport pattern.

In comparison to the NCAR results, the meridional heat transport is higher in all MIAMI experiments (Fig. 7b). Mixing in those experiments takes place predominantly along isopycnals. Any explicitly prescribed diapycnal mixing (Table 1) has only a minor diminishing effect on the maximum heat transport, as shown by the results of MIAMI-3. Omission of diapycnal mixing in that experiment increased the annual mean maximum value of heat transport to 1.3 PW, versus 1.2 PW in MIAMI-1. The more notable difference in the heat transport patterns of MIAMI-1 and MIAMI-3 can be seen in the 10°S–10°N latitude band, where the transport in MIAMI-3 is almost twice that of MIAMI-1.

This may be related to the fact that diapycnal mixing is an important factor in the strength and configuration of the equatorial region circulation, as noted above in relation to the EUC (section 3c). The MIAMI-2 experiment demonstrates that without relaxation toward Levitus (1982) in the Labrador Sea, the maximum heat transport drops slightly to 1.1 PW. Finally, omission of relaxation to climatology at the southern and northern walls as well as in the Labrador Sea and Mediterranean regions, in both the NCAR and MIAMI simulations, decreased the annual mean maximum to less than 0.4 PW (not illustrated).

While the annual mean northward heat transport in the model results depends heavily upon proper replication of the vertical/meridional flow, seasonal variations in that transport are primarily a wind-driven effect and show little dependence upon boundary conditions or mixing parameterizations (Böning and Herrmann 1994). The winter maximum and summer minimum in heat transport across 8°N, associated with the seasonal reversal of the North Equatorial Countercurrent (Philander and Pacanowski 1986), are well reproduced in both the NCAR and MIAMI results. Böning and Herrmann (1994) note that the annual range of heat transport across that latitude in various CME experiments is sensitive to both the grid resolution and the wind stress used. Though the annual mean heat transport at 8°N is 30% larger in the MIAMI experiments, the 1.5 PW range observed in the NCAR results at 8°N approximately equals the range seen in MIAMI (Fig. 8), both models being forced by the same wind stress data (Hellerman and Rosenstein 1983).

Little observational data regarding the seasonal cycle of heat transport across 8°N is available. In the subtropics, however, Molinari et al. (1990) have reported the annual cycle of heat transport across 26.5°N as ranging from 0.69 PW in February to 1.86 PW in July. This estimate is considerably larger than the amplitude seen in the NCAR or MIAMI results at that latitude (Fig. 8).

b. Overturning cell

Until the introduction of the GM90 eddy parameterization, spurious upwelling inshore of the western boundary current in the North Atlantic was identified as one of the major flaws of numerical simulations performed with the GFDL model (Toggweiler 1994; Böning et al. 1995). This is illustrated in Fig. 9a, which displays the annual mean meridional overturning streamfunction for NCAR-1. The strong upwelling observed at midlatitudes significantly reduces the amount of deep water carried toward the equator from the source regions. This translates into a smaller meridional heat transport than observed, as discussed in the previous section. The overturning pattern for NCAR-2, which uses the traditional Laplacian mixing, differs little from that of NCAR-1 and is therefore not illustrated. However, as discussed in Böning et al. (1995), adoption of the isopycnal advection and mixing parameterization of GM90 yields substantial improvements in the overturning rate (about 13 Sv of NADW reach the southern boundary in NCAR-3 versus only 8 Sv in NCAR-1 and NCAR-2) (Fig. 9b) and heat transport (1 PW in NCAR-3 versus 0.7 PW in NCAR-1 and NCAR-2) (Fig. 7a). In all NCAR cases, the maximum overturning rate is ~18 Sv, in good agreement with observations (Schmitz 1995).

Just as the eddy-induced circulation is introduced in the depth coordinate model by the GM90 parameterization, it is incorporated in MICOM by smoothing the isopycnal surfaces (section 2). In all MIAMI runs initialized from climatology, the overturning rate is strong (21 Sv in MIAMI-1, 19 Sv in MIAMI-2, and 22 Sv in MIAMI-3; Fig. 10) and there is no loss of deep water due to upwelling in midlatitudes (a minimum of 18 Sv

TABLE 2. September averaged layer thicknesses (rounded to the next meter) corresponding to the potential density values of section 2 for Levitus (1982) climatology, NCAR-1 (year 240), NCAR-3 (year 284), MIAMI-1 (year 20), and MIAMI-4 (year 20).

Layer	σ_θ	Levitus	NCAR-1	NCAR-3	MIAMI-1	MIAMI-4
2	24.70	16	18	17	19	19
3	25.28	19	20	23	17	17
4	25.77	22	25	29	25	25
5	26.18	33	40	38	42	44
6	26.52	79	61	54	65	65
7	26.80	96	94	80	86	83
8	27.03	122	117	116	127	119
9	27.22	153	150	154	173	167
10	27.38	161	161	160	170	159
11	27.52	145	171	164	159	157
12	27.64	161	194	201	163	168
13	27.74	298	381	395	261	304
14	27.82	546	927	1250	558	705
15	27.88	1027	1169	872	1022	1244
16	27.92	673	30	7	632	243

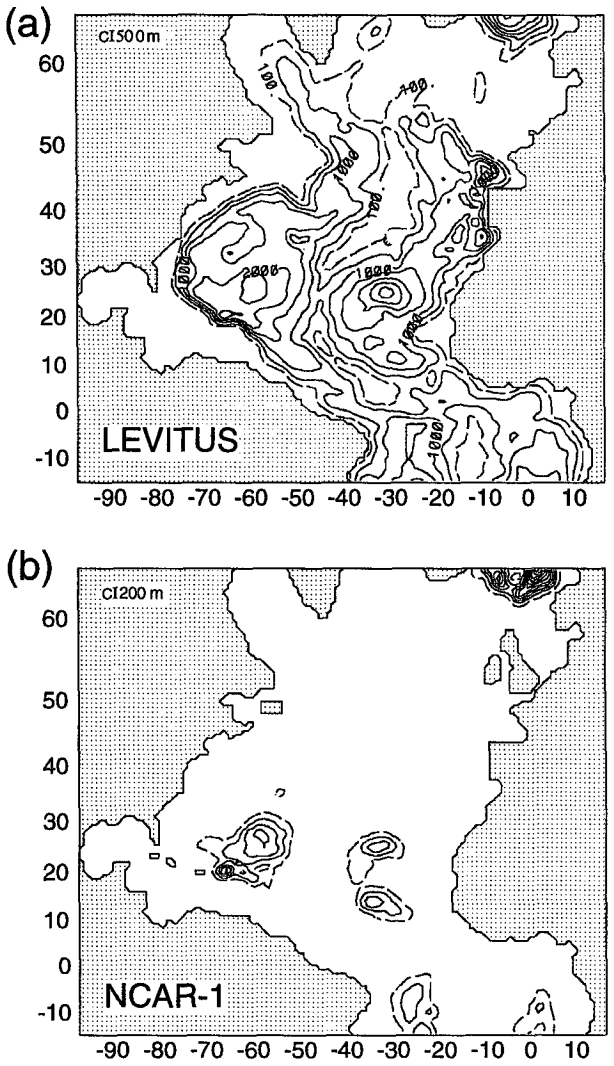

FIG. 11. Layer 16 (σ_θ = 27.92) thickness derived from the Levitus (1982) climatology (CI = 500 m) and from year 240 of NCAR-1 (CI = 200 m).

of NADW reach the southern boundary in all runs). In contrast to observational estimates (Schmitz 1995) suggesting a relatively constant thermohaline throughflow, the southward transport in the MIAMI experiments increases slightly from the midlatitudes to the Tropics. (Note that for display purposes, the MIAMI results have been transformed to x, y, z coordinate space in Fig. 10.)

The most striking difference in the overturning patterns of the NCAR and MIAMI results is the rather small southward transport, less than 5 Sv, below 3000 m in the NCAR simulations versus more than 10 Sv present in all MIAMI simulations. In both NCAR-1 and NCAR-2, a cell of the opposite sign is present below 3000 m, generally attributed to the penetration of Antarctic Bottom Water (AABW) into the North Atlantic. The transport associated with the observed AABW cell in the North Atlantic is small, on the order of a few Sverdrups (Schmitz 1995). While one would expect this cell to be represented in the numerical simulations, since dense AABW is prescribed in the southern buffer zone, its existence appears to be directly correlated to the strength of the overturning circulation. The AABW cell is almost nonexistent in NCAR-3 (Fig. 9b) where the NADW reaches the southern boundary. In an experiment carried out by Döscher et al. (1994) (Fig. 9c), identical to NCAR-1 except for the use of the Isemer and Hasse (1987) wind stress climatology and relaxation to a northern buffer zone based on an actual hydrographic section, the AABW cell completely disappears. The southward transport of NADW in the tropical latitudes reaches 16 Sv in the Döscher et al. (1994) simulation, as compared to 8 Sv in NCAR-1. In the MIAMI simulations, no transport cell of opposite sign is present (Fig. 10), as the southward transport of NADW in the tropical latitudes is on the order of 20 Sv. A strong southward transport in the MIAMI experiments is likely due to the fact that the integrations performed with MICOM allow the retention of properties of dense flows as they cross the system of deep North Atlantic ridges (Roberts et al. 1996). This will be discussed in more detail in section 5.

The role of the Labrador Sea in the formation of NADW in the MIAMI runs is illustrated in the overturning streamfunction of MIAMI-2 (Fig. 10b), in which the relaxation toward Levitus (1982) was turned off in the Labrador region (Fig. 1). The contribution from the Labrador Sea to the production of deep water and to the vertical/meridional transport in MIAMI-2 is small (less than 2 Sv), in agreement with the results of CME experiments analyzed by Böning et al. (1996). Neither model is able to represent the two observed deep water paths, one originating in the Labrador Sea and one in the Norwegian and Greenland Seas (Roemmich and Wunsch 1985; Fine and Molinari 1988; Rhein et al. 1995). This is likely due, as surmised by Döscher et al. (1994), to inadequacies in the specification of the buffer zones and/or to lack of vertical resolution.

The maximum overturning rates seen in both the NCAR and MIAMI results are not seriously out of line when compared to various observational estimates given for the transport of the NADW cell (e.g., Roemmich and Wunsch 1985; Schmitz and McCartney 1993; Schmitz 1995), ranging from 13 to 20 Sv. In both models, the specification of thermohaline boundary conditions from smoothed climatology may significantly affect the magnitude of the model overturning and heat transport (Döscher et al. 1994).

5. Time evolution of water masses

That the NCAR and MIAMI results differ substantially in the meridional overturning streamfunction pattern leads us to investigate the time evolution of dif-

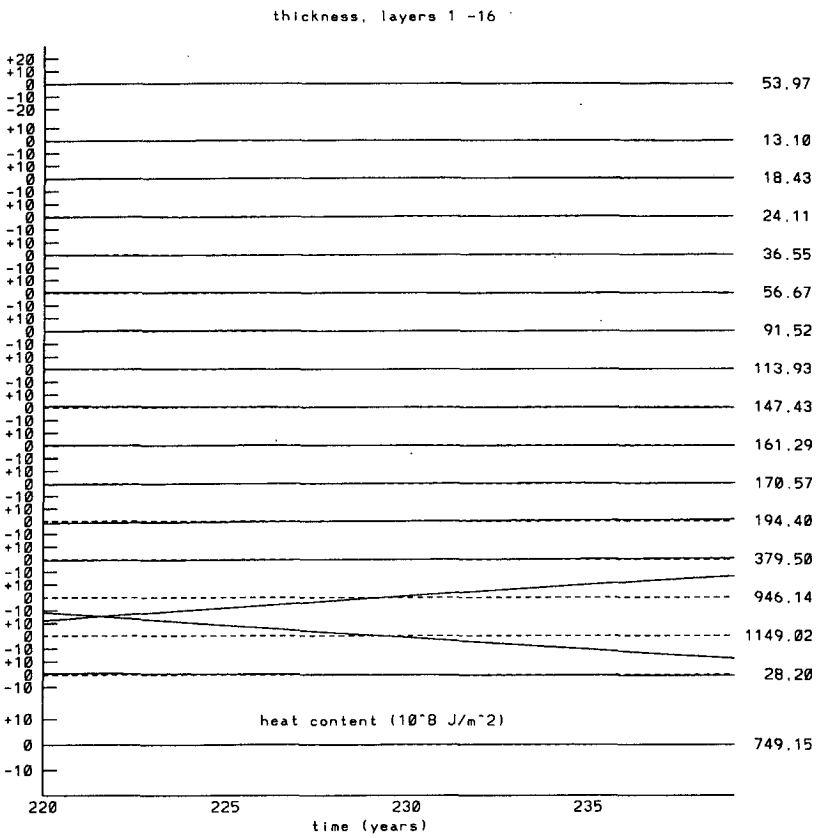

FIG. 12. Twenty-year time evolution of the domain-averaged layer thicknesses (for the mixed layer and the 15 isopycnic layers) and of the domain averaged heat content (bottom curve) computed for the month of September for NCAR-1, beginning from year 220.

ferent water masses in the experiments. Furthermore, we wish to address the question raised in the introduction, namely: What is the rate of divergence between an isopycnic coordinate model and a depth coordinate model, given the same initial conditions?

In order to address this subject, we monitor in time the amount of mass present in each layer. We first look at the end state of NCAR-1 and MIAMI-1 in comparison to the initial state, defined by the Levitus (1982) climatology. The domain-averaged layer thicknesses for the 15 isopycnic layers below the mixed layer, computed for the month of September, are presented in Table 2 for several experiments. Multiplied by the domain area, they provide an indication of the volume occupied by water of the density corresponding to each layer. A major difference in the mass of layer 16 is immediately seen in the figures of Table 2. In NCAR-1, the layer has almost completely vanished (~30 m average thickness; Fig. 11b), in comparison to Levitus (1982) climatology (~675 m; Fig. 11a) and MIAMI-1 (~630 m; Fig. 14a).

A 20-year time evolution of the September averaged layer thicknesses is presented in Figs. 12 and 13 for NCAR-1 and MIAMI-1. (Only the September averaged layer thicknesses are plotted in order to filter out the seasonal cycle. The month of September was chosen since it corresponds to the seasonal minimum in mixed layer depth.) The bottom curve of Figs. 12 and 13 shows the time evolution of the heat content, defined as

$$\rho c_p \sum hT\Delta x\Delta y / \sum \Delta x\Delta y \quad (\text{units of J m}^{-2}), \quad (1)$$

where $\rho = 1000$ kg m^{-3}, $c_p = 3990$ J kg^{-1} K^{-1}, T is the temperature, h is the layer thickness, $\Delta x\Delta y$ is the grid cell area, and the sums are taken over all grid points and all layers. In NCAR-1, which was first integrated for 220 years, there is little change in the final 20 years, indicating thermal equilibrium. MIAMI-1, on the other hand, shows an overall increase in heat content. Both heat contents are of the same average magnitude ($\sim 750 \times 10^8$ J m^{-2}). If one focuses on the evolution of layers 15 and 16 in NCAR-1, there is a decrease in mass in layer 15 and almost no change in layer 16, which has nearly vanished as mentioned above (Table 2, Fig. 12). This means that the highest-density water masses are being depleted in this run. In MIAMI-1, a decrease in mass is observed in layer 16, while

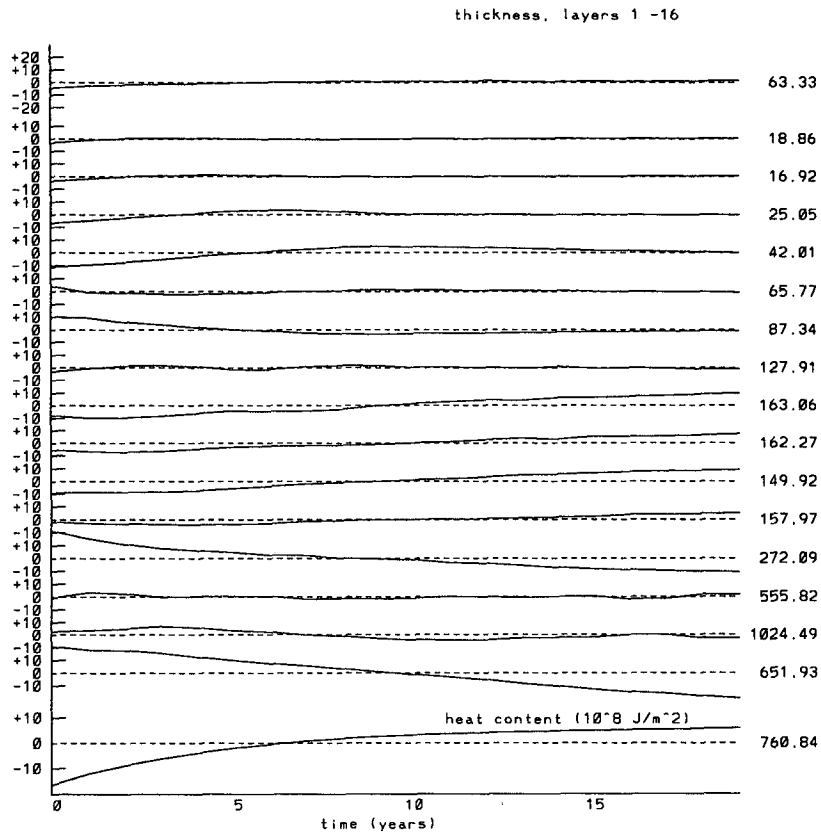

FIG. 13. As in Fig. 12 but for MIAMI-1 for years 1–20.

several midlayers increase in mass and layer 15 remains stable (Fig. 13).

Since MIAMI-1 was integrated for only 20 years from Levitus (1982) climatology, one may ask if the lower layer will continue decreasing in mass to approach that of NCAR-1 after more than 200 years. In theory, relaxation in the buffer zones toward observed densities should keep a certain amount of high-density water everywhere in the domain as it is advected away from the boundaries. In order to address this issue, MICOM was initialized from year 220 of NCAR-1, which exhibits a nearly nonexistent layer 16 as illustrated by Fig. 11b, and then integrated for 20 years (MIAMI-4). In that time span, the thickness of layer 16 of MIAMI-4 jumps from an average of 30 to 240 m (Fig. 14c, Table 2), as the dense water present in the buffer zones is advected into the domain interior along the major topographic features. The layer 16 domain-averaged thickness has not yet stabilized at the end of 20 years (Fig. 15), nor has it reached a level equivalent to that shown in the climatology (Fig. 11a, Table 2). The domainwide thickness of the layer also does not allow for any exchange of mass between the eastern and western basins at the Gibbs Fracture Zone as occurs in MIAMI-1 (Fig. 14).

Finally, a similar layer census (not illustrated) was performed for NCAR-3, which used the GM90 mixing parameterization and was initialized from the final state of NCAR-1. The average thickness for layer 16 at the end of the integration (year 284) was found to be somewhat lower than in NCAR-1, on the order of 10 m (Table 2). This is in agreement with Böning et al. (1995) who report that the addition of the GM90 parameterization to their CME experiment (NCAR-3) led to only a minor change in net deep-water production in the subpolar North Atlantic. This result seems to be at variance with the work of Hirst and McDougall (1996), in which the parameterization of eddy-induced advection allowed the dense polar-shelf fluid to flow down the topography and along the ocean floor with minimal diffusion.

6. Summary and discussion

The results of two numerical ocean models using two different vertical coordinates (depth and density) have been compared. The models were configured as similarly as possible considering the intrinsic nature of each. The comparison has emphasized the impact of

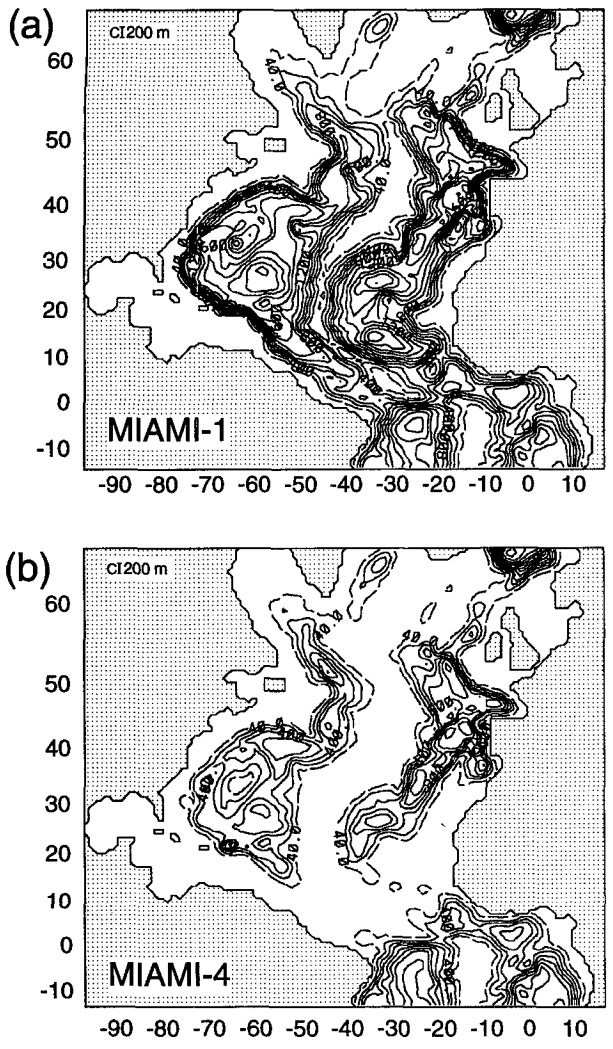

FIG. 14. Layer 16 (σ_θ = 27.92) thickness fields for MIAMI-1 and MIAMI-4 in September of year 20. CI = 200 m.

varying mixing parameterizations on the models' behavior. Simulations performed with a depth coordinate numerical model utilizing the GM90 parameterization of the eddy-induced circulation have been compared to simulations using an isopycnic coordinate numerical model that does not require such a parameterization in order to achieve along-isopycnal mixing.

The overall agreement in the horizontal flow patterns between the NCAR and MIAMI experiments is not surprising in the subtropical gyre, where one expects the Sverdrup balance to dominate and the vertical discretization and associated mixing to be relatively unimportant. On the other hand, greater differences might have been expected in the subpolar gyre where higher order effects [joint effect of baroclinicity and relief (JEBAR), mixing, mixed layer physics, . . .] become important (Bryan et al. 1995a), and where weak stratification leads to vertical resolution problems in an isopycnic coordinate framework. Some of the differences in the results can be accounted for by differences in the setup of the two models. That the model equations are solved on a C grid in MICOM versus a B grid in the GFDL model was shown in section 3a to be responsible for the difference in transport in the Straits of Florida. This difference may decrease with an increase in vertical and horizontal resolution, which would provide a better representation of the topography. The regular mesh on a Mercator projection of MICOM provides higher grid resolution away from the equator than the spherical grid used in the NCAR experiments and may contribute to the stronger ventilation patterns seen in the MIAMI experiments. An additional model difference is that in the NCAR experiments discussed in this paper, only the tracers are mixed along isopycnal surfaces, while momentum mixing still possesses a significant cross-isopycnal component (Table 1). In MICOM, mixing of both tracers and momentum takes place along isopycnals.

In both models, the equatorial undercurrent is a robust feature with a core velocity in the MICOM simulations roughly double that of the NCAR results. In agreement with previous numerical simulations, diapycnal mixing was shown to play an important role in controlling the EUC strength. Adoption of the GM90 parameterization, on the other hand, had a negligible impact on the EUC dynamics.

The most counterintuitive result of the comparison exercise is the weakening of the ventilation patterns in the results of NCAR-3 (Fig. 6). In that case, using the GM90 mixing parameterization, one might have expected a better agreement with the MIAMI simulations. This matter is presently under investigation in a series of sensitivity experiments using the GFDL model with different values of the isopycnal diffusivity coefficient.

The overturning streamfunction patterns in the NCAR runs incorporating the GM90 mixing parameterization agree with the MICOM results in that the spurious midlatitude upwelling seen in earlier NCAR runs is not present (Böning et al. 1995). Mixing is predominantly along isopycnals in MICOM and an effect equivalent to the GM90 parameterization is included in the form of smoothing of the isopycnic surfaces. The overturning circulation in MICOM is stronger in all cases than the overturning produced in the NCAR model runs, even those without spurious midlatitude upwelling. Accordingly, the maximum annual northward heat transport in the MICOM results is stronger than that seen in the NCAR runs.

The most striking difference between the two numerical models is brought out by the discussion in section 5 of the temporal evolution of water masses corresponding to different density classes. In order to reveal how the water mass properties in a CME high-resolution experiment drift away from the initially prescribed state, Klinck (1995) has discussed the tem-

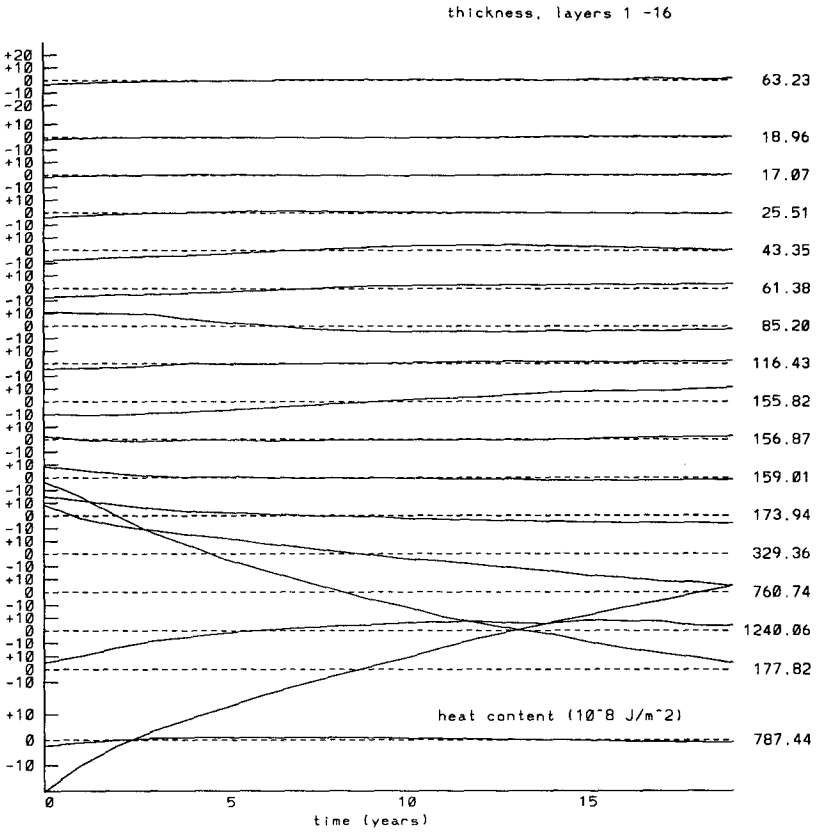

FIG. 15. As in Fig. 12 but for MIAMI-4.

poral evolution of model T–S structure. This analysis, however, does not easily show the change in model density structure or the major difference between the two numerical models compared here, namely, the inability of the GFDL model to retain its densest water masses after long integration periods, despite the presence of buffer zones in which temperature and salinity are restored to climatology (Levitus 1982). Inclusion of the GM90 mixing parameterization led to only minor changes in net deep-water production.

Dense overflows in depth coordinate models are known to mix vigorously with the surrounding warmer, saltier water so that their properties change relatively quickly as they cross the complex system of North Atlantic ridges (Gerdes 1993; Roberts et al. 1996; Roberts and Wood 1996, manuscript submitted to *J. Phys. Oceanogr.*). Specifically, heavy water overflowing a ridge is unable to translate its negative buoyancy into a downward velocity component quickly enough to avoid vertical homogenization by the model's convective adjustment mechanism. In layer models such as MICOM, on the other hand, dense overflows always follow the bottom and thus do not lead to static instability and excessive vertical mixing. One improvement for depth-coordinate simulations might be the inclusion of plume models to better represent the spreading of dense water (Jungclaus and Backhaus 1994).

The original CME was intended as a reference experiment and as such used fairly simple parameterizations and forcing functions. While these simplifications may affect the realism of the solution, they do allow for a relatively fair comparison between numerical models. They also leave room for improvement, as shown by the many sensitivity studies that have been performed with the GFDL model since the original design (Holland and Bryan 1994a; Döscher et al. 1994; Beckman et al. 1994; Böning et al. 1995, . . .). Döscher et al. (1994) and Klinck (1995) point out the inadequacies of buffer zones that restore the T and S fields to climatology in an attempt to recover the vertical shear of the currents through geostrophic adjustment. Döscher et al. (1994) show that restoration in the northern buffer zone to T and S based on a hydrographic section observed at one particular time rather than on climatological conditions brings about a much stronger signal of the Denmark Strait overflow water (almost nonexistent in the Levitus climatology) as well as a stronger southward transport at the lower NADW level (Fig. 9c). Klinck (1995), in a detailed analysis of the high resolution CME (Bryan and Holland 1989),

concludes that the water masses created by the buffer zones do not compare well with observations and that part of the problem resides in the smoothed nature of the climatology. While the sensitivity of the GFDL model to different boundary conditions is relatively well documented in the literature (Holland and Bryan 1994a; Döscher et al. 1994), more sensitivity studies are needed with MICOM.

In conclusion, for the configuration discussed in this paper, the model-generated fields viewed at specific times in the integration of the two experiments do not appear to strongly depend on the particular model architecture and are in good agreement with one another. However, given the same initial conditions, the integrated properties of the depth coordinate model and the isopycnic coordinate model diverge significantly in time, primarily due to the depth coordinate model's inability to retain its densest water masses after long integration periods.

Acknowledgments. Discussions with W. Johns, J. Klinck, T. McDougall, D. Olson, C. Rooth, and K. Speer proved timely and valuable. Support was provided by the National Science Foundation through Grant OCE-9206643. Computations were carried out using the CRAY Y-MP at the National Center for Atmospheric Research (NCAR). NCAR is sponsored by the National Science Foundation.

REFERENCES

Beckmann, A., C. W. Böning, C. Köberle, and J. Willebrand, 1994: Effects of increased horizontal resolution in a simulation of the North Atlantic Ocean. *J. Phys. Oceanogr.*, **24,** 326–344.

Blanke, B., and P. Delecluse, 1993: Variability of the tropical Atlantic Ocean simulated by a general circulation model with two different mixed-layer physics. *J. Phys. Oceanogr.*, **23,** 1363–1388.

Bleck, R., and E. P. Chassignet, 1994: Simulating the oceanic circulation with isopycnic-coordinate models. *The Oceans: Physical–Chemical Dynamics and Human Impact.* S. K. Majumdar, E. W. Miller, G. S. Forbes, R. F. Schmalz, and A. A. Panah, Eds., The Pennsylvania Academy of Science, 17–39.

——, C. Rooth, D. Hu, and L. T. Smith, 1992: Salinity-driven transients in a wind- and thermohaline-forced isopycnic coordinate model of the North Atlantic. *J. Phys. Oceanogr.*, **22,** 1486–1505.

——, S. Dean, M. O'Keefe, and A. Sawdey, 1995: A comparison of data-parallel and message-passing versions of the Miami Isopycnic Coordinate Ocean Model (MICOM). *Parallel Computing,* **21,** 1695–1720.

Böning, C. W., and R. G. Budich, 1992: Eddy dynamics in a primitive equation model: Sensitivity to horizontal resolution and friction. *J. Phys. Oceanogr.*, **22,** 1271–1289.

——, and P. Herrmann, 1994: Annual poleward heat transport in the ocean. Results from high-resolution modeling of the North and equatorial Atlantic. *J. Phys. Oceanogr.*, **24,** 91–105.

——, R. Döscher, and H.-J. Isemer, 1991a: Monthly mean wind stress and Sverdrup transports in the North Atlantic: A comparison of the Hellerman–Rosenstein and Isemer–Hasse climatologies. *J. Phys. Oceanogr.*, **21,** 221–235.

——, ——, and R. G. Budich, 1991b: Seasonal transport variation in the western subtropical North Atlantic: Experiments with an eddy-resolving model. *J. Phys. Oceanogr.*, **21,** 1271–1289.

——, W. R. Holland, F. O. Bryan, G. Danabasoglu, and J. C. McWilliams, 1995: An overlooked problem in model simulations of the thermohaline circulation and heat transport in the Atlantic Ocean. *J. Climate,* **8,** 515–523.

——, F. O. Bryan, W. R. Holland, and R. Döscher, 1996: Thermohaline circulation and poleward heat transport in a high-resolution model of the North Atlantic. *J. Phys. Oceanogr.,* in press.

Bryan, F. O., and W. R. Holland, 1989: A high resolution simulation of the wind- and thermohaline-driven circulation in the North Atlantic Ocean. *Parameterization of Small-Scale Processes. Proc. Aha Huliko'a Hawaiian Winter Workshop,* P. Muller and D. Anderson, Eds., University of Hawaii, 99–115.

——, C. W. Böning, and W. R. Holland, 1995a: On the midlatitude circulation of a high-resolution model of the North Atlantic. *J. Phys. Oceanogr.*, **25,** 289–305.

——, I. Wainer, and W. R. Holland, 1995b: Sensitivity of the tropical Atlantic circulation to specification of wind stress climatology. *J. Geophys. Res.*, **100,** 24 729–24 744.

Bryan, K., 1984: Accelerating the convergence to equilibrium of ocean-climate models. *J. Phys. Oceanogr.*, **14,** 666–673.

Bryden, H. D., and M. M. Hall, 1980: Heat transport by currents across 25°N latitude in the Atlantic Ocean. *Science,* **207,** 884–886.

Cox, M. D., 1984: A primitive equation three-dimensional model of the ocean. NOAA Tech. Rep. 1, GFDL/NOAA, Princeton University, N.J., 144 pp.

——, 1987: Isopycnal diffusion in a *z*-coordinate ocean model. *Ocean Modeling,* **74,** 1–5.

Döscher, R., C. W. Böning, and P. Herrmann, 1994: Response of circulation and heat transport in the North Atlantic to changes in thermohaline forcing in northern latitudes. A model study. *J. Phys. Oceanogr.*, **24,** 2306–2320.

Fine, R. A., and R. L. Molinari, 1988: A continuous deep western boundary current between Abaco (26.5°N) and Barbados (13°N). *Deep-Sea Res.*, **35,** 1441–1450.

Garzoli, S. L., and E. J. Katz, 1983: The forced annual reversal of the Atlantic North Equatorial countercurrent. *J. Phys. Oceanogr.*, **13,** 2082–2093.

Gent, P. R., and J. C. McWilliams, 1990: Isopycnal mixing in ocean circulation models. *J. Phys. Oceanogr.*, **20,** 150–155.

——, J. Willebrand, T. J. McDougall, and J. C. McWilliams, 1995: Parameterizing eddy-induced tracer transports in ocean circulation models. *J. Phys. Oceanogr.*, **25,** 463–474.

Gerdes, R., 1993: A primitive equation ocean circulation model using a general vertical coordinate transformation. Part II: Application to an overflow problem. *J. Geophys. Res.*, **98,** 14 702–14 726.

Han, Y.-J., 1984: A numerical world ocean general circulation model. Part II: A baroclinic experiment. *Dyn. Atmos. Oceans,* **8,** 141–172.

Hellerman, S., and M. Rosenstein, 1983: Normal monthly wind stress over the world ocean with error estimates. *J. Phys. Oceanogr.*, **13,** 1093–1104.

Hirst, A. C., and T. J. McDougall, 1996: Deep water properties and surface buoyancy flux as simulated by a *z*-coordinate model including eddy-induced advection. *J. Phys. Oceanogr.*, **26,** 1320–1343.

Holland, W. R., and P. Rhines, 1980: An example of eddy-induced ocean circulation. *J. Phys. Oceanogr.*, **10,** 1010–1031.

——, and F. O. Bryan, 1994a: Sensitivity studies on the role of the ocean in climate change. *Ocean Processes in Climate Dynamics: Global and Mediterranean Examples,* P. Malanotte-Rizzoli, and A. R. Robinson, Eds., Kluwer, 111–134.

——, and ——, 1994b: Modeling the wind and thermohaline circulation in the North Atlantic Ocean. *Ocean Processes in Climate Dynamics: Global and Mediterranean Examples,* P. Malanotte-Rizzoli and A. R. Robinson, Eds., Kluwer, 135–156.

Iselin, C. O., 1939: The influence of vertical and lateral turbulence on the characteristics of the waters at mid-depth. *Trans. Amer. Geophys. Union,* **20,** 414–417.

Isemer, H. J., and L. Hasse, 1987: *The Bunker Climate Atlas of the North Atlantic Ocean.* Vol. 2, *Air–Sea Interactions,* Springer-Verlag, 256 pp.

Jungclaus, J. H., and J. O. Backhaus, 1994: Application of a transient reduced gravity plume model to Denmark Strait Overflow. *J. Geophys. Res.,* **99,** 12 375–12 396.

Klinck, J. M., 1995: Thermohaline structure of an eddy-resolving North Atlantic model. The influence of boundary conditions. *J. Phys. Oceanogr.,* **25,** 1174–1195.

Levitus, S., 1982: *Climatological Atlas of the World Ocean.* NOAA Prof. Paper No. 13, U.S. Govt. Printing Office, 173 pp.

Luyten, J. R., J. Pedlosky, and H. Stommel, 1983: The ventilated thermocline. *J. Phys. Oceanogr.,* **13,** 292–309.

Marsh, R., M. J. Roberts, R. A. Wood, and A. L. New, 1996: An intercomparison of a Bryan-Cox type ocean model and an isopycnic ocean model. Part II: The subtropical gyre and meridional heat transport. *J. Phys. Oceanogr.,* **26,** 1528–1551.

Marshall, J. C., A. J. G. Nurser, and R. G. Williams, 1993: Inferring the subduction rate and period over the North Atlantic. *J. Phys. Oceanogr.,* **23,** 1315–1329.

McCartney, M. S., and L. D. Talley, 1982: The subpolar mode water of the North Atlantic. *J. Phys. Oceanogr.,* **12,** 1169–1188.

McDougall, T. J., and J. A. Church, 1986: Pitfalls with the numerical representation of isopycnal and diapycnal mixing. *J. Phys. Oceanogr.,* **16,** 196–199.

——, and P. C. McIntosh, 1996: The temporal-residual-mean velocity. Part I: Derivation and the scalar conservation equations. *J. Phys. Oceanogr.,* in press.

McWilliams, J. C., 1996: Modeling the oceanic general circulation. *Annu. Rev. Fluid Mech.,* **28,** 215–248.

Molinari, R. L., E. Johns, and J. Festa, 1990: The annual cycle of meridional heat flux in the Atlantic Ocean at 26.5°N. *J. Phys. Oceanogr.,* **20,** 476–482.

Montgomery, R. B., 1940: The present evidence on the importance of lateral mixing processes in the ocean. *Bull. Amer. Meteor. Soc.,* **21,** 87–94.

New, A. L., R. Bleck, Y. Jia, R. Marsh, M. Huddleston, and S. Barnard, 1995: An isopycnic model study of the North Atlantic. Part I: Model experiment. *J. Phys. Oceanogr.,* **25,** 2667–2699.

Philander, G., and R. C. Pacanowski, 1986: A model of the seasonal cycle in the tropical Atlantic Ocean. *J. Geophys. Res.,* **91,** 14 192–14 206.

Qiu, B., and R. X. Huang, 1995: Ventilation of the North Atlantic and North Pacific: Subduction versus obduction. *J. Phys. Oceanogr.,* **25,** 2374–2390.

Redi, M. H., 1982: Oceanic isopycnal mixing by coordinate rotation. *J. Phys. Oceanogr.,* **12,** 1154–1158.

Rhein, M., L. Stramma, and U. Send, 1995: The Atlantic deep western boundary current. Water masses and transports near the equator. *J. Geophys. Res.,* **100,** 2441–2458.

——, R. Marsh, A. L. New, and R. A. Wood, 1996: An intercomparison of a Bryan-Cox type ocean model and an isopycnic ocean model. Part I: The subpolar gyre and high-latitude processes. *J. Phys. Oceanogr.,* **26,** 1495–1527.

Roemmich, D., and C. Wunsch, 1985: Two transatlantic sections. Meridional circulation and heat flux in the subtropical North Atlantic Ocean. *Deep-Sea Res.,* **32,** 619–664.

Schmitz, W. J., Jr., 1995: On the interbasin-scale thermohaline circulation. *Rev. Geophys.,* **33,** 151–173.

——, and M. S. McCartney, 1993: On the North Atlantic circulation. *Rev. Geophys.,* **31,** 29–49.

Schott, F. A., and C. W. Böning, 1991: The WOCE model in the Western Equatorial Atlantic: Upper layer circulation. *J. Geophys. Res.,* **96,** 6993–7004.

——, T. N. Lee, and R. Zantopp, 1988: Variability of structure and transport of the Florida Current in the period range of days to seasonal. *J. Phys. Oceanogr.,* **18,** 1209–1230.

Toggweiler, J. R., 1994: The ocean's overturning circulation. *Phys. Today,* **47**(11), 45–50.

U.S. WOCE Office, 1993: U.S. WOCE Implementation Plan. U.S. WOCE Office, College Station, TX, 146 pp.

Veronis, G., 1975: The role of models in tracer studies. *Numerical Models of Ocean Circulations,* Natl. Acad. Sci., 133–146.

Wacongne, S., 1989: Dynamical regimes of a fully nonlinear stratified model of the Atlantic Equatorial Undercurrent. *J. Geophys. Res.,* **94,** 4801–4815.

Williams, R. G., M. A. Spall, and J. C. Marshall, 1995: Does Stommel's mixed layer "demon" work? *J. Phys. Oceanogr.,* **25,** 3089–3102.